HIGH SCHOOL EDITION
Journal of Student Research
Volume 11 Issue 2 (2022)

Classifying Alzheimer's Disease with Machine Learning via Wavelet Transform Subband Combinations

ABSTRACT

The 3-D wavelet transform has been used with machine learning techniques to help identify Alzheimer's Disease (AD) and Mild Cognitive Impairment (MCI) through magnetic resonance imaging (MRI). Although this approach resulted in high accuracy, a large number of subband permutations were obtained due to the usage of the 3-D wavelet transform, which causes redundancy and computational inefficiency during classification. To address this issue, this study discovers the combination with the minimum subbands giving a comparable accuracy with the original approach that used all subbands. The Alzheimer's Disease Neuroimaging Initiative (ADNI) was used to gain de-identified MRI scans for classification with 75% training and 25% test scans. The scans were standardized by pre-processing through skull stripping, segmentation, and smoothing using the MATLAB toolboxes Statistical Parametric Mapping 12 (SPM 12) and Computation Anatomy Toolbox 12 (CAT 12). Feature extraction was then completed through different 3-D wavelet transform subband combinations. Support vector machine (SVM) classification was used with radial basis function kernels (RBF) to screen patients for AD, MCI, or cognitively normal (CN) status 3 times per subband combination. The mean and standard deviation of the test accuracy for each combination were recorded. Among the tested combinations, the maximum mean test accuracy was 95.3%. To prevent overfitting, five-fold cross-validation was performed on the top 40% subband combinations based on the mean test accuracy. The maximum cross-validation accuracy is 97.3%. Therefore, this study shows the potential of using less 3-D wavelet transform subbands to help screen patients for AD or MCI in the future.

Introduction

Alzheimer's Disease (AD) is a progressive neurodegenerative condition that leads to brain mass loss and significantly affects the quality of life for patients and their families (National Institute on Aging, 2019). It is classified as the most common dementia that manifests in humans (National Institute on Aging, 2019), and its prevalence in the United States of America is expected to more than double by 2050 unless any breakthrough regarding prevention or cure happens (Alzheimer's Association, 2021). Mild Cognitive Impairment (MCI) is a transitional stage in cognitive function from natural cognitive decline to AD (Henderson, n.d.). Patients with MCI are at high risk for conversion to AD and the progression of further cognitive decline (National Institute on Aging, 2019). Diagnosis of MCI and AD has primarily centered on cognitive tests administered by a physician or through brain scans, such as MRI scans (National Institute of Neurological Disorders and Stroke, 2022).

In addition to conventional methods, machine learning techniques including support vector machine (SVM), artificial neural network (ANN), deep learning (DL), and ensemble methods have shown promise identifying AD and MCI (Tanveer et al., 2020). Among them, SVM classification is one of the most excellent methods (Zhang et al., 2015) because it is able to produce high levels of classification accuracy without knowledge about the geometry and distribution of the given dataset (Cortes & Vapnik, 1995). SVM selects and optimizes a hyperplane to separate data (Bhasin & Agrawal, 2020) by maximizing the margin, or the distance from the hyperplane to the closest data points. SVM functions that separate the data (called kernels) can either be linear or non-linear (Cortes & Vapnik, 1995). However, researchers stated that SVM methods that use non-linear kernels perform well on non-linear data such as MRI scans (Zhang et al., 2015). In SVM and other machine learning classifiers, cross-validation is a procedure used to test the predictive power of a classifier on data that has not been used in the classifier before (Wang et al., 2014). In essence, it tests to make sure a classifier can generalize well and does not overfit a dataset. In k-fold cross-validation, the data set is broken into k folds, with $k-1$ folds being used as training data and then iterating the process

While cross-validation validates SVM results, robust SVM classification itself relies on effective feature extraction. One type of feature extraction that has been used with SVMs in identifying AD and MCI is the wavelet transform, a type of transform that allows for the capture of both frequency and temporal information from a signal (Mallat, 1989). Past studies using the wavelet transform have produced promising results (Bhasin & Agrawal, 2020; Wang et al., 2014; Mishra and Deepthi, 2020; Jha et al., 2017). For example, (Bhasin & Agrawal, 2020) was able to achieve 88.34% classification accuracy for identifying MCI against cognitively normal (CN) scans. However, these

studies suffered from only using a few 2-D slices of MRI scans to reduce run time and then applied the 2-D wavelet transform to those slices, which may result in missing foci of AD (Jha et al., 2017). In addition to the 2-D wavelet transform applications, applications of the 3-D wavelet transform have been performed, such as (Mishra & Deepthi, 2020), where they combined several different types of the wavelet transform such as the dual tree M-band wavelet transform or the stationary wavelet transform and then classified the data with an SVM classifier. Researchers also used the wavelet transform on 3D MRI scans followed by principal component analysis and feature fusion before final SVM classification (Ayaz et al., 2017). However, these procedures use all wavelet transform subbands, inevitably adding time to feature extraction. Subbands are created because the wavelet transform applies a low-pass (approximation coefficient creating) and high-pass (detail coefficient creating) filter in each dimension (Kai, n.d.). Figure 1 displays how subbands are created from a 3-D MRI scan. To be more specific, there are two subbands for a 1-D signal, four for a 2-D image, and eight for a 3-D image. These subbands differ in what filters have been applied in each dimension, meaning the data encoded in them is different and each subband will act different in an SVM classifier. Although the studies have demonstrated the potential of using all the subbands in AD and MCI identification, the efficacy of just using some subbands for classification is a question that needs to be answered.

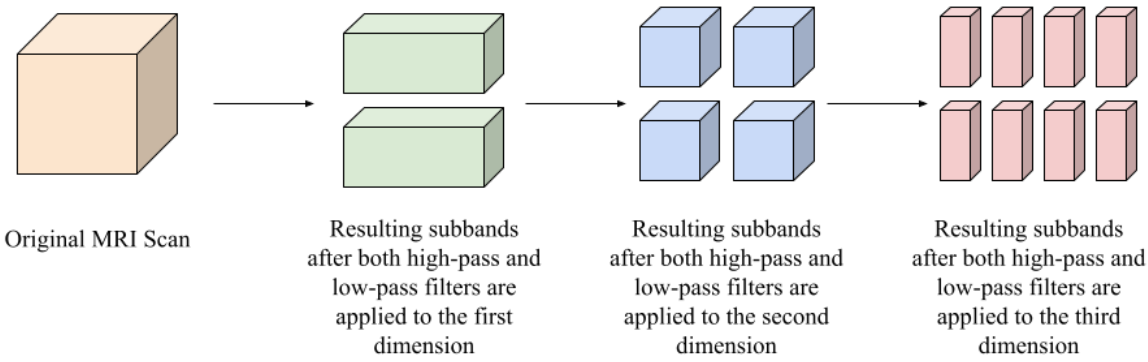

Figure 1. As high-pass and low-pass filters are applied to each dimension, a 3-D MRI scan gets divided into eight different subbands.

This study presents a machine learning solution based on selecting 3-D wavelet subband combinations of two and using a SVM method for classifying MRI scans as AD, MCI, or CN. By only using two subbands, the run time was significantly reduced while a comparable accuracy was achieved compared to past studies using all the subbands from the 3-D wavelet transform.

Methodology

Data Acquisition

The ADNI database was used in this research, which consists of scans from MRI, positron emission tomography (PET), and other data relating to biomarkers of AD (ADNI, 2009). The objective of the database has been to test the utility of using these biomarkers to characterize the status and progression of MCI and AD (ADNI, 2009). The database has four sections: ADNI-1, ADNI-GO, ADNI-2, and ADNI-3. The ADNI-1 part of the dataset was used because it was the easiest to obtain due to it being well-established, with each 3-D scan from the section falling into three categories: AD, MCI, and CN. Only 50 scans from each category were selected due to computational limitations. As a result, this is a pilot study. The scans were selected by increasing numerical value of the file identification. 75% of these scans were used for training while 25% were used for test classification.

Each of the MRI scans were downloaded in the NIFTI format, which stores them in an accessible manner by the computer. A comma separated values (CSV) spreadsheet provided by ADNI was used to move the images into folders based on their subject condition (AD, MCI, or CN).

Image Pre-processing

Gray matter atrophy has been found to be responsible for MCI and AD progression (Apostolova et al., 2007). Pre-processing also standardizes the images. (Friston et al., 1994). Thus, pre-processing via segmentation and smoothing to capture just the gray matter of the MRI scans is necessary. The MRI scans were segmented using the Computational Anatomy Toolbox 12 (CAT 12) (Rajapakse et al., 1997) toolbox of MATLAB. These programs segmented the MRI images into grey matter, white matter, and cerebrospinal fluid. Figure 2 shows an unmodified MRI and a segmented MRI, which demonstrates the differences between them. After segmentation, the grey matter from each MRI scan was smoothed using the Statistical Parametric Mapping 12 (SPM12) (Friston et al, 1994) toolbox of MATLAB. These smoothed grey matter images were then sent for feature extraction.

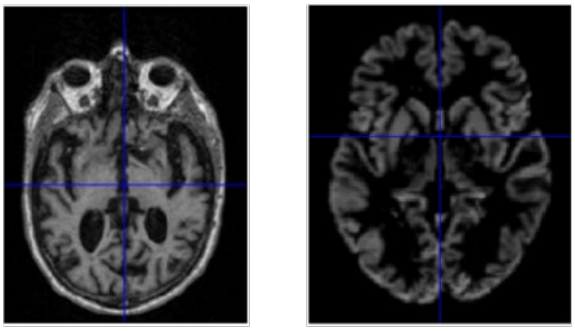

A) B)

Figure 2. Pre-processing via SPM12 produces an MRI image without the skull and only containing gray matter: 2A) An unmodified MRI scan; and 2B) The MRI scan after segmentation.

Feature Extraction

The wavelet transform is a process by which both the frequency and time information of a signal can be captured, which applies well for non-stationary signals and images like MRIs (Wang et al., 2014). Types of wavelet transforms can be sectioned into two categories based on the orthogonality of the mother wavelet: continuous wavelet transform (CWT), which uses non-orthogonal mother wavelets, and discrete wavelet transform (DWT), which uses orthogonal mother wavelets. Since MRI scans are discrete, DWT is used in MRI classification (Bhasin & Agrawal, 2020). Equation 1 represents the wavelet expansion of a discrete function $f(x)$

$$f(x) = \frac{1}{\sqrt{A}}\sum_{a} W_{\tau}(P,a)\tau_{P,a}(x) + \frac{1}{\sqrt{A}}\sum_{p=1}^{P}\sum_{a} W_{\psi}(p,a)\psi_{p,a}(x) \quad (1)$$

where $\frac{1}{\sqrt{A}}$ is the normalizing factor, P is the decomposition level, $\psi_{p,a}(x)$ represents the wavelet coefficients, and $\tau_{P,a}(x)$ represents scaling coefficients. $\psi_{p,a}(x)$ and $\tau_{P,a}(x)$ are discrete functions in and where $a = \{0, 1, 2, \ldots \frac{A}{2^P} - 1\}$. Equations 2 and 3 show how the wavelet and scaling coefficients are generated (Bhasin & Agrawal, 2020):

$$W_{\psi}(p,a) = \frac{1}{\sqrt{A}}\sum_{x=0}^{A-1} f(x)\widetilde{\psi_{(p,a)}}(x) \quad (2)$$

$$W_{\tau}(P,a) = \frac{1}{\sqrt{A}}\sum_{x=0}^{A-1} f(x)\widetilde{\tau_{(P,a)}}(x) \quad (3)$$

To display how the DWT performs on an MRI scan, the 2-D DWT performed on a 2-D slice of a 3-D MRI scan. Four subbands were generated by a low-pass or high-pass filter being performed on each of the two dimensions in 2-D image. Each subband is represented as a two-letter key, representing what subbands are in which dimension. An "a" represents an approximation subband produced by a low-pass filter and a "d" represents a detail subband produced by a high-pass filter. Figure 2 shows the four resulting subbands after this procedure.

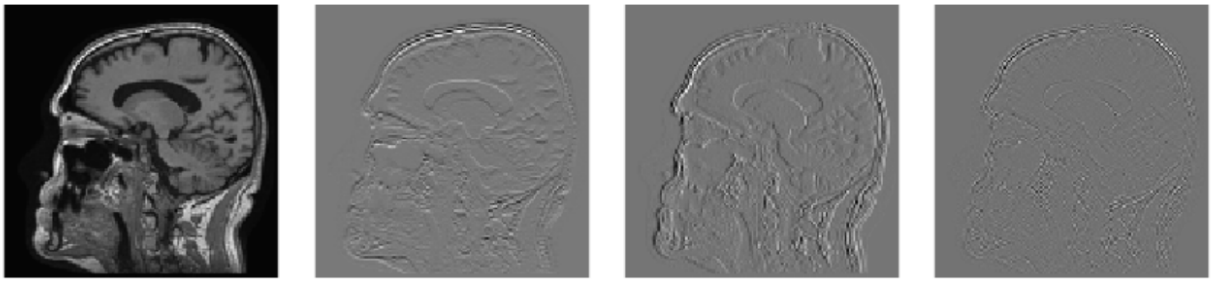

A) B) C) D)

Figure 2. The visualization of the 2-D DWT performed on a model slice with all four subband patterns: 2A: Approximation subbands in both dimensions (aa); 2B: approximation subbands in the horizontal dimension and detail subbands in the vertical dimension (ad); 2C: Detail subbands in the horizontal dimension and approximation coefficients in the vertical dimension (da); 2D: Detail subbands in both dimensions (dd).

However, the application of the DWT on 2-D slices of MRI scans is prone to missing foci of AD pathology that are necessary for accurate classification (Jha et al., 2017).

The application of the 3-D DWT was the primary focus of this study for its use in feature extraction of the entire 3-D MRI while only using certain subband combinations. After pre-processing, each scan was taken and resized into a standardized size. From there, the 3-D DWT was executed using the biorthogonal 1.3 wavelet with the PyWavelets package (access the PyWavelets documentation at https://pywavelets.readthedocs.io/en/latest/) of Python 3.9.6. Different subband combinations were selected and stored for later classification. To get multiple information points but limit the amount of computational capacity needed to calculate the classification, each subband combination consisted of two of the eight possible subbands at the 3-D level, resulting in a total of 36 subband combinations.

Classification and Cross-Validation

The classification of the final features in this experiment was done by a SVM classifier. Each subband combination was classified three separate times with the SVM. The C value, or regularization parameter, was ten in all trials, and the tolerance was 1×10^{-3}. Since linear SVMs do not perform well on non-linear data (Zhang et al., 2015), non-linear radial basis function (RBF) kernels were used. The test classification accuracy was recorded each time the subband combination was run through the SVM. The mean and standard deviation (SD) of the test accuracies for each subband combination were then calculated.

The top 40% of the subband combinations by mean test accuracy were selected for cross-validation. Five-fold cross-validation was used to validate the performance of these combinations.

Results and Discussion

After the 3-D DWT was performed on 150 MRI scans, the feature extracted scans were run through a SVM classifier with RBF kernels and C-value of 10 three times per subband combination. The test classification accuracy was measured for each of the three runs, and then the mean and SD of the test classification accuracies were calculated. Each subband is represented by a three-letter key detailing whether there is an approximation subband (produced by a low-pass filter) or a detail subband (produced by a high-pass filter) in the x, y, and z dimensions. An "a" represents an approximation subband and a "d" represents a detail subband. Table 1 shows the mean and SD of

the test accuracy for three runs per subband combination. The minimum mean test accuracy was 75.2% and the maximum mean test accuracy was 95.7%.

The top 40% of subband combinations sorted by mean test accuracy were selected for five-fold cross-validation. Table 2 shows the mean and SD of cross-validation accuracy per subband combination, which are sorted by highest mean cross-validation accuracy and lowest SD. Five-fold cross-validation of the selected subband combinations yielded a minimum mean accuracy of 91.3% and a maximum of 97.3%.

Table 1. The mean and SD of the test accuracy for three runs each, shown as (mean ± SD). The bolded accuracies were selected for cross-validation.

aaa	0.855 ± 0.030							
aad	0.872 ± 0.032	0.889 ± 0.030						
ada	0.863 ± 0.015	**0.934 ± 0.061**	**0.923 ± 0.044**					
add	0.752 ± 0.074	**0.940 ± 0.030**	**0.923 ± 0.026**	0.897 ± 0.051				
daa	0.838 ± 0.030	0.906 ± 0.059	0.897 ± 0.068	0.897 ± 0.051	0.855 ± 0.116			
dad	0.812 ± 0.015	**0.940 ± 0.015**	**0.940 ± 0.059**	0.889 ± 0.053	0.863 ± 0.097	**0.940 ± 0.030**		
dda	0.803 ± 0.039	**0.949 ± 0.068**	**0.949 ± 0.026**	**0.949 ± 0.051**	0.915 ± 0.053	0.915 ± 0.015	**0.923 ± 0.027**	
ddd	0.863 ± 0.090	**0.957 ± 0.053**	**0.923 ± 0.077**	0.915 ± 0.126	**0.923 ± 0.051**	0.906 ± 0.065	0.897 ± 0.077	0.880 ± 0.074
	aaa	**aad**	**ada**	**add**	**daa**	**dad**	**dda**	**ddd**

Table 2. The mean and SD of cross-validation accuracy for five-fold cross-validation, shown as (mean ± SD).

Subband Combination	Mean and SD of Cross-Validation Accuracy
aad, add	0.973 ± 0.013
dda, dda	$0.967 \pm 1.1 \times 10^{-6}$
ada, add	0.960 ± 0.033
ada, dad	0.960 ± 0.033
aad, ada	0.953 ± 0.045
ada, dda	0.953 ± 0.050
ada, ddd	0.953 ± 0.050
aad, dad	0.947 ± 0.039
add, dda	0.947 ± 0.054
daa, ddd	0.940 ± 0.053
aad, dda	0.920 ± 0.068
ada, ada	0.920 ± 0.068
dad, dad	0.913 ± 0.016
aad, ddd	0.913 ± 0.039

This study found that the selection of only two subband patterns can still produce accurate classification. The maximum cross-validation classification accuracy was 97.3%, compared to the 76.0% accuracy found by Ayaz et al. or the 92.8% accuracy found by Sujatha Kumari et al. (Sujatha Kumari et al., 2021). This means that despite using less subbands and needing less computational power, this study's procedure was able to produce better classification results than previous proposed methods using the 3-D DWT. These results show that the use of only a

few subbands in specific subband combinations may be a viable innovation to increase the efficiency of screening patients for AD or MCI via MRI.

Further research is required to see if the method used in this study is applicable to larger data sets. In addition, it is possible the accuracy can be further increased by using a convolutional neural network (CNN) as the classifier.

Conclusion

This study finds that the use of only certain subband combinations may be a viable solution to creating a more efficient method of 3-D DWT on MRI scans to classify patient cognitive status as AD, MCI, or CN. The maximum mean test classification accuracy was 95.7% from the "aad, ddd" subband combination, and the maximum five-fold cross-validation accuracy was 97.3% from the "aad, add" subband combination. Despite requiring less computation capacity and less steps, these results were better than previous proposed procedures to screen patients for AD or MCI based on performing the 3D-DWT on MRI scans. This result shows that using a limited 3D-DWT subband method may be able to increase the efficiency of classifying patients for AD or MCI with MRI. However, this procedure needs to be validated on larger sample sizes of MRI scans.

Acknowledgements

I would like to thank Xiangyi Cheng for her mentorship and guidance of me through this project.

References

ADNI | About. (2009). Usc.edu. http://adni.loni.usc.edu/about/

Ayaz, A., Ahmad, M. Z., Khurshid, K., & Kamboh, A. M. (2017). MRI based automated diagnosis of Alzheimer's: Fusing 3D wavelet-features with clinical data. *2017 39th Annual International Conference of the IEEE Engineering in Medicine and Biology Society (EMBC)*. https://doi.org/10.1109/embc.2017.8037048

Apostolova, L. G., Steiner, C. A., Akopyan, G. G., Dutton, R. A., Hayashi, K. M., Toga, A. W., Cummings, J. L., & Thompson, P. M. (2007). Three-Dimensional Gray Matter Atrophy Mapping in Mild Cognitive Impairment and Mild Alzheimer Disease. *Archives of Neurology*, *64*(10), 1489. https://doi.org/10.1001/archneur.64.10.1489

Bhasin, H., & Agrawal, R. K. (2020). A combination of 3-D discrete wavelet transform and 3-D local binary pattern for classification of mild cognitive impairment. *BMC Medical Informatics and Decision Making*, *20*(1). https://doi.org/10.1186/s12911-020-1055-x

Cortes, C., & Vapnik, V. (1995). Support-vector networks. *Machine Learning*, *20*(3), 273–297. https://doi.org/10.1007/bf00994018

Facts and Figures. (2021). Alzheimer's Disease and Dementia. https://www.alz.org/alzheimers-dementia/facts-figures#prevalence

Friston, K. J., Holmes, A. P., Worsley, K. J., Poline, J.-P. ., Frith, C. D., & Frackowiak, R. S. J. (1994). Statistical parametric maps in functional imaging: A general linear approach. *Human Brain Mapping*, *2*(4), 189–210. https://doi.org/10.1002/hbm.460020402

Henderson, V. (n.d.). *Mild Cognitive Impairment*. Retrieved February 15, 2022, from https://med.stanford.edu/content/dam/sm/adrc/documents/adrc-information-sheet-mild-cognitive-impairment.pdf

Jha, D., Kim, J.-I., & Kwon, G.-R. (2017). Diagnosis of Alzheimer's Disease Using Dual-Tree Complex Wavelet Transform, PCA, and Feed-Forward Neural Network. *Journal of Healthcare Engineering*, *2017*, 1–13. https://doi.org/10.1155/2017/9060124

Kai, S., Li, K., & Selesnick, I. (n.d.). *Wavelet Software at Brooklyn Poly*. Eeweb.engineering.nyu.edu. Retrieved February 8, 2022, from https://eeweb.engineering.nyu.edu/iselesni/WaveletSoftware/standard3D.html

Leifer, B. P. (2003). Early diagnosis of Alzheimer's disease: clinical and economic benefits. *Journal of the American Geriatrics Society*, *51*(5 Suppl Dementia), S281-288. https://doi.org/10.1046/j.1532-5415.5153.x

Mallat, S. G. (1989). A theory for multiresolution signal decomposition: the wavelet representation. *IEEE Transactions on Pattern Analysis and Machine Intelligence*, *11*(7), 674–693. https://doi.org/10.1109/34.192463

Mishra, S. K., & Deepthi, V. H. (2020). Brain image classification by the combination of different wavelet transforms and support vector machine classification. *Journal of Ambient Intelligence and Humanized Computing*, *12*(6), 6741–6749. https://doi.org/10.1007/s12652-020-02299-y

National Institute on Aging. (2019, May 22). *Alzheimer's Disease Fact Sheet*. National Institute on Aging. https://www.nia.nih.gov/health/alzheimers-disease-fact-sheet

Rajapakse, J. C., Giedd, J. N., & Rapoport, J. L. (1997). Statistical approach to segmentation of single-channel cerebral MR images. *IEEE Transactions on Medical Imaging*, *16*(2), 176–186. https://doi.org/10.1109/42.563663

Sujatha Kumari, B. A., Yadiyala, A. G. V., Aruna, B. J., Radha, C., & Shwetha, B. (2021). Early Detection of Mild Cognitive Impairment Using 3D Wavelet Transform. *Data Intelligence and Cognitive Informatics*, 445–455. https://doi.org/10.1007/978-981-15-8530-2_36

Tanveer, M., Richhariya, B., Khan, R. U., Rashid, A. H., Khanna, P., Prasad, M., & Lin, C. T. (2020). Machine Learning Techniques for the Diagnosis of Alzheimer's Disease. *ACM Transactions on Multimedia Computing, Communications, and Applications*, *16*(1s), 1–35. https://doi.org/10.1145/3344998

The Dementias: Hope Through Research | National Institute of Neurological Disorders and Stroke. (n.d.). Www.ninds.nih.gov. Retrieved January 29, 2022, from https://www.ninds.nih.gov/Disorders/Patient-Caregiver-Education/Hope-Through-Research/Dementia-Hope-Through-Research#diagnosis

Wang, X., Nan, B., Zhu, J., & Koeppe, R. (2014). Regularized 3D functional regression for brain image data via Haar wavelets. *The Annals of Applied Statistics*, *8*(2). https://doi.org/10.1214/14-aoas736

Ye, D. H., Pohl, K. M., & Davatzikos, C. (2011). Semi-supervised Pattern Classification: Application to Structural MRI of Alzheimer's Disease. *2011 International Workshop on Pattern Recognition in NeuroImaging*, 1–4. https://doi.org/10.1109/prni.2011.12

Zhang, Y., Dong, Z., Phillips, P., Wang, S., Ji, G., Yang, J., & Yuan, T.-F. (2015). Detection of subjects and brain regions related to Alzheimer's disease using 3D MRI scans based on eigenbrain and machine learning. *Frontiers in Computational Neuroscience*, *9*. https://doi.org/10.3389/fncom.2015.00066